JOURNAL OF MAGNETIC RESONANCE **84,** 554–572 (1989)

Dynamic Imaging of Diffusion by ESR

JOZEF K. MOSCICKI,* YEON-K. SHIN, AND JACK H. FREED

Baker Laboratory of Chemistry, Cornell University, Ithaca, New York 14853-1301

Received December 5, 1988; revised February 22, 1989

A comprehensive analysis of the accuracy and reliability of dynamic imaging of diffusion by ESR is presented. The importance of analyzing the data in Fourier space is emphasized, and a new method which enables the determination of the important Fourier modes while also providing a test of the reliability of the measurement of the diffusion coefficient, D_x, is presented. It is shown that values of $D_x \sim 10^{-9}$ cm^2 s^{-1} can be measured in about one hour to 10–20% accuracy, whereas for $D_x \sim 10^{-7}$ cm^2 s^{-1} the error should be below 1%. These statements are applicable for experiments in which there is unrestricted diffusion, and an initial Gaussian concentration profile. Systematic error resulting from non-Gaussian concentration profiles is shown to be relatively unimportant. However, the finite sweep time through a spectrum is found to yield a systematic error analogous to a Doppler shift, which tends to cancel only for the case of unrestricted diffusion. The experimental geometry in which there is diffusion from a reflective boundary requires special adjustments to align the gradient-on and -off spectra. A convenient and reliable method to accomplish this is presented. Nevertheless, there are inherently greater sources of error for this geometry, and this is confirmed by the experimental results. Utilizing the reflective boundary geometry, the longitudinal and transverse diffusion coefficients for PD-TEMPONE (^{15}N labeled) in the nematic phase of MBBA at 20°C are 3.7×10^{-7} and 2.5×10^{-7} cm^2 s^{-1}, respectively. Their ratio of 1.5 is consistent with results for other probe molecules in MBBA.

The technique of dynamic imaging of diffusion by ESR (DID-ESR) has been developed in the last few years, and it has already proved to be very useful in the measurement of diffusion coefficients in fluids including normal liquids, liquid crystals, and model membranes (*1–3*). In our initial work (*1*), we showed that by utilizing a quasi-one-dimensional sample with an inhomogeneous distribution of spin probes dissolved in a fluid solvent, one may image this concentration distribution as a function of time by employing a magnetic field gradient along the axis of diffusion, and thereby observe the approach to a homogeneous distribution via translational diffusion. From the time variation of the concentration distribution, one obtains the diffusion coefficient, D_x. However, such experiments required a long time to obtain D_x (e.g., 5–7 days for $D_x \approx 10^{-6}$ cm^2 s^{-1}). More recently (*2*), major improvements to the technique which enable much more rapid measurement were made (e.g., $D_x \approx 10^{-8}$ cm^2 s^{-1} may be measured in about one hour), and these improvements also enabled us to reduce the influence of several complicating features of the original experiment (e.g., spatial variation of the sensitivity of ESR cavity). This resulted from two ad-

* On sabbatical leave from Institute of Physics, Jagiellonian University, Krakow, Poland.

0022-2364/89 $3.00

vances. First, one must prepare a distribution of spin probes which is highly localized in the center of microwave cavity, so that the concentration profile will change significantly in a short time and this change will take place in the region where the sensitivity of the cavity is quite homogeneous. Second, the imaging results are analyzed in Fourier space (inverse wavelength space). This overcomes difficulties that reduce the accuracy in measurement of the concentration profiles in real space, and perhaps even more important, the diffusion equation is easily analyzed in inverse wavelength space such that only those Fourier components with sufficient sensitivity to the diffusion need be included.

The Fourier-domain analysis was shown to be applicable to two basic experimental geometries, one in which there are no boundary conditions and spin probes diffuse freely in both directions from a source (i.e., "unrestricted diffusion") and the second in which there is diffusion from a source placed at the reflective boundary ("restricted diffusion") (*2*). The former geometry was found particularly user-friendly and a special virtue of DID-ESR was realized in our recent study of lateral diffusion in model membranes (*3*), wherein we showed that one can simultaneously study translational diffusion and rotational diffusion from the same set of ESR spectra. This led to new and interesting correlations between ordering and dynamics.

Our experience in the past was that the geometry of restricted diffusion is fraught with greater experimental problems and is thus inherently more difficult for obtaining accurate results. We have found experimentally (*2*) that a precise alignment of the reflecting wall at the center of the ESR cavity is needed in order to simplify the numerical data analysis. If this condition is not fulfilled, then one must use cumbersome data manipulation to estimate the diffusion coefficient, leading to much higher uncertainties in the result. Our further efforts confirmed this difficulty.

We continued the search for a reliable improvement in the analysis of the data from the restricted diffusion geometry and this paper reports on our latest findings. We propose a new technique for the restricted diffusion experiment. The technique does not require perfect alignment of the reflective wall in the center of the cavity. We will show that the effects of perfect alignment are equivalent either to appropriately varying the static magnetic field between recording gradient-*on* and -*off* spectra or to numerically shifting recorded spectra. We find that, with the improvements proposed, the restricted diffusion experiment, although slightly more challenging experimentally, provides a dependable method for studying translation diffusion. Additionally, the new numerical analysis of the data that we use can also be used in the unrestricted diffusion experiment; it clarifies the accuracy of the DID-ESR method by enabling a simple assessment of the relevant Fourier modes.

There are a number of matters relating to the accuracy and reliability of DID-ESR which were not addressed in the previous work. The objective of this paper is also to present a comprehensive discussion of the accuracy and reliability of DID-ESR. As a result of these considerations we have learned how to improve the data analysis and how to deal with residual artifacts that could otherwise limit the accuracy of this experiment. What emerges from the present study is that DID-ESR in both geometries, unrestricted and restricted, is indeed a highly reliable and very accurate method for determining diffusion coefficients of probes and allows the effects of virtually all of the experimental artifacts that could limit its accuracy to be suppressed.

The paper is organized as follows. In the first section we review the basic principles of the DID-ESR experiment and introduce a scaling of variables useful for understanding the new numerical procedure of handling the restricted diffusion data and for simplifying the evaluation of the accuracy and reliability of DID-ESR.

In the second section in this work, we consider, in some detail, new improvements in the DID-ESR technique. We introduce a new way of data handling and illustrate this procedure with some experimental results. We discuss the basic modifications of the restricted diffusion experiment and show how the new data handling helps to achieve this.

In the next to last section in this work, we show how the new insights provided by our present analysis enable us to estimate the minimum measurable D_x and the accuracy of the measurement. We find that the two experimental geometries should be considered separately, although there are many points in common. We find that with present experimental techniques the smallest D_x obtainable is $D_{\min} \approx 10^{-9}$ cm^2 s^{-1} in a 1 h (or *rapid*) experiment, provided there is unrestricted diffusion and an initial Gaussian concentration profile. Of course, correspondingly smaller values of D_x may be achieved by increasing the length of the experiment. The error in D_x can be very small, e.g., below 1% for 10^{-7} cm^2 s^{-1}, in the case of unrestricted diffusion. Somewhat greater error is found for diffusion from a reflective boundary.

Concluding remarks appear in the last section.

BASIC CONCEPTS OF THE EXPERIMENT

The DID-ESR experiment is specifically designed for studying two simple cases of the diffusion: (**I**) *unrestricted diffusion* in opposite directions from an instantaneous source, and (**II**) *restricted diffusion* only in one direction from an instantaneous source, i.e., diffusion from the source located at an impermeable reflective boundary (*1–2*). Monitoring the time evolution of the concentration distribution of spin probes is done with the aid of a one-dimensional uniform magnetic field gradient. The ESR spectrum recorded in the presence of the magnetic field gradient (gradient-on spectrum), $I_g(B, t)$, is a result of the convolution of the hyperfine spectrum of the spin probe (gradient-off spectrum), $I_0(B)$, with the concentration of spin probes $C(x, t)$ (*1, 2*),

$$I_g(B, t) = C * I_0 = \int_{-\infty}^{\infty} C(B', t) I_0(B - B') dB', \qquad [1]$$

since the magnetic field gradient $\nabla_x B$, maps x onto $B_j B = x \nabla_x \mathrm{B}$, and the concentration of spin probes at any point in the sample is low enough for Heisenberg spin exchange (HSE) not to occur (*1, 2*).

The simplicity of the DID-ESR experiment is in the fact that we are monitoring solely the component of diffusion in the direction of the one-dimensional field gradient, even though the sample is three-dimensional.

Considerations become especially easy when the concentration of spin probes is low enough for the translational diffusion along x to obey Fick's second law (*4*),

$$\frac{\partial C(x,t)}{\partial t} = D_x \frac{\partial^2 C(x,t)}{\partial x^2}, \qquad [2]$$

where D_x is the diffusion constant, and $C(x, t)$ is the concentration of spin probes ("concentration profile") along x at time t. In practice, preparing the initial concentration of spin probes low enough to obey Fick's law but still high enough to provide a strong ESR signal (without HSE broadening) is not a problem (*1–3*). Case (**I**) would then correspond to a situation where a small amount of the spin-probe-enriched material is initially confined to the center of a quasi-one-dimensional sample, e.g., capillary tube. If a very narrow source [i.e., one that can be considered a point source ($\equiv\delta$ function)] is placed at $x = 0$ at $t = 0$, then the solution of Eq. [2] at later time t takes the form of

$$C(x,t) = \frac{C_0}{\sqrt{4\pi D_x t}} \exp\left\{-\left(\frac{x}{\sqrt{4D_x t}}\right)^2\right\}. \qquad [3]$$

In practice, however, the initial distribution extends over a finite distance, and may not be Gaussian. If $C(x, 0)$ is the initial concentration profile, then the concentration profile at some later time t can be written down as

$$C(x,t) = \frac{1}{\sqrt{4\pi D_x t}} \int_{-\infty}^{\infty} C(x', t=0) e^{-(x-x')^2/4D_x t} dx', \qquad [4]$$

i.e., the convolution of the initial distribution with a Gaussian function, $G(x; 2D_x t) = (4\pi D_x t)^{-1/2} e^{-x^2/4D_x t}$.

Case (**II**) corresponds to a situation where the source material is confined at the initial time to the vicinity of the reflecting wall, which conveniently could be either the bottom or the wall of the ESR sample cell. The boundary (reflective) condition, $(\partial C/\partial x)|_{x=0} = 0$, introduces a symmetry such that Eq. [3] will also describe the evolution of concentration profile from the point source placed at the boundary, but with C_0 being replaced by $2C_0$ and x space restricted to positive values (*4*). Equation [4] may also be easily adapted to the case of a reflecting wall at $x = 0$ (*4*).

Prior to outlining the main points of the data analysis, we wish to emphasize a useful scaling of the distance, x, and magnetic field, B, introduced by the recording procedure of ESR spectra. This scaling renders x and B formally equivalent which simplifies the mathematical description of the experiment.

First, a uniform one-dimensional magnetic field gradient, $B' = \nabla_x B$, which is used to map the concentration profile from x space onto B space (see Eq. [1]), effectively scales the distance by B' so the variables become $\xi_B = x \cdot B'$ and $D_B = D_x \cdot B'^2$. Second, the ESR spectrum is detected by sweeping the magnetic field over some range, say, B_s. Thus, the magnetic field is scaled with $1/B_s$ and the scaled variables become $\xi = x \cdot B'/B_s$ and $D_\xi = D_x \cdot (B'/B_s)^2$, so ξ is dimensionless and D_ξ is in units of inverse time. It follows directly from the last scaling[1] that the dimensionless distance and

[1] It is interesting to note that, after additional scaling of the time with D_ξ, i.e., $\tau \equiv D_\xi \cdot t$, the diffusion equation in dimensionless space (ξ, τ) takes a very simple form:

$$\frac{\partial C(\xi,\tau)}{\partial \tau} = \frac{\partial^2 C(\xi,\tau)}{\partial \xi^2}.$$

magnetic field are equivalent: $B/B_s = x \cdot B'/B_s = \xi$. Thus, the ESR spectrum and the concentration profile become functions of the same variables, and we will capitalize on this property in the restricted diffusion experiment. The particular property of this scaling is that basic equations of DID-ESR (i.e., Eqs. [1]–[4]) hold also for the scaled variables, which can easily be verified by substituting the new variables into Eqs. [1]–[4]. Therefore, we may use scaled variables without losing the general character of the following discussion.

The Fourier transform of Eq. [4] yields

$$\mathcal{C}(\kappa, t) = \mathcal{C}(\kappa, 0)\exp\{-4\pi^2 D_\xi t \kappa^2\} \qquad [5]$$

or,

$$\ln\{\mathcal{C}(\kappa, t)\} = -4\pi^2 D_\xi t \kappa^2 + \ln\{\mathcal{C}(\kappa, 0)\}, \qquad [6]$$

where $\mathcal{C}(\kappa, t)$ is the Fourier-space image of $C(\xi, t)$ and κ is the inverse wavelength in dimensionless units. The latter equation can be used directly to analyze data from unrestricted diffusion in Fourier space. We notice that essentially two $\mathcal{C}(\kappa, t)$, recorded at distinct times, t_i and t_j, are sufficient to determine D_ξ,

$$\ln\left[\frac{\mathcal{C}(\kappa, t_i)}{\mathcal{C}(\kappa, t_j)}\right] = -4\pi^2 D_\xi \Delta t_{ij} \kappa^2, \qquad [7]$$

where $\Delta t_{ij} = t_i - t_j$. The linear least-squares fit with respect to $\Delta t_{ij}\kappa^2$ (cf. Eq. [7]) to the experimental data yields the slope $-4\pi^2 D_\xi$, and thus D_ξ. In practice, to increase the precision of D_ξ, a number of concentration profiles at different times, $i = 1, \ldots, N$, are recorded (*2, 3*). Then, first, the concentration profiles at different times are *paired* and, with aid of Eq. [7], the slope $-4\pi^2 D_\xi \Delta t_{ij}$ is determined for each pair (*step one*). Next, these slopes are analyzed as a function (linear) of Δt_{ij}, resulting in D_ξ (*step two*) (*2*). Note that, in principle, steps one and two can be merged, since one can directly perform the linear least-squares fit of Eq. [7] to experimental data with respect to $\Delta t_{ij}\kappa^2$. Doing so, however, one must be careful: as explained in our previous paper (*2*), in step one the intercept of the linear fit for each pair $\{i, j\}$ is an order of magnitude larger than the slope and this might bias the final result. In order to compensate for this, the intercept for each pair should be subtracted prior to further analysis.

Finally, D_ξ is converted to real-space units:

$$D_x = D_\xi \cdot (B_s/B')^2. \qquad [8]$$

Deconvolution of the concentration profile from $I_g(\xi, t)$ requires special comments. It follows from Eq. [1] that because the FT of I_g is just the product of two individual FTs, the extraction of the concentration profile in inverse wavelength space merely requires a division of two complex functions. If $\mathcal{I}_g(\kappa, t)$ and $\mathcal{I}_0(\kappa)$ are the Fourier transforms of $I_g(\xi, t)$ and $I_0(\xi)$, respectively, then

$$\mathcal{C}(\kappa, t) = \mathcal{I}_g(\kappa, t)/\mathcal{I}_0(\kappa). \qquad [9]$$

For the general case of unrestricted diffusion, expressing $\mathcal{C}(\kappa, t)$, $\mathcal{I}_0(\kappa)$, and $\mathcal{I}_g(\kappa)$

in polar form, $|\mathcal{C}(\kappa, t)|e^{2\pi j\phi_{\kappa,t}}$, $|\mathcal{I}_0(\kappa)|e^{2\pi j\phi_0}$, and $|\mathcal{I}_g(\kappa)|e^{2\pi j(\phi_0+\phi_{\kappa,t})}$, respectively, ($j = \sqrt{-1}$), and substituting into Eq. [7] yield

$$\ln\left\{\frac{|\mathcal{C}(\kappa, t_i)|}{|\mathcal{C}(\kappa, t_j)|}\right\} = \ln\left\{\frac{|\mathcal{I}_g(\kappa, t_i)|}{|\mathcal{I}_g(\kappa, t_j)|}\right\} = -4\pi^2 D_\xi t\kappa^2 \qquad [10]$$

and $\phi_{\kappa,t_i} = \phi_{\kappa,t_j} = \text{const}$. Clearly, all the information about the shape of a concentration profile is contained in the amplitude of $\mathcal{I}_g(\kappa, t)$. In fact $\mathcal{I}_0(\kappa)$ cancels out of Eq. [10], and therefore $I_0(\xi)$ is not required. This also means that the relative positions of either C or I_0 on the ξ scale are irrelevant since

$$C(\xi - \xi_0, t) * I_0(\xi - \xi_i) \overset{\text{FT}}{\longleftrightarrow} \mathcal{C}(\kappa, t)e^{2\pi j\xi_0\kappa} \cdot \mathcal{I}_0(\kappa)e^{2\pi j\xi_i\kappa}$$
$$= [|\mathcal{C}(\kappa, t)|e^{2\pi j(\xi_0+\xi_i)\kappa}] \cdot \mathcal{I}_0(\kappa), \qquad [11]$$

where ξ_0 and ξ_i are the center positions of the concentration profile and of I_0 on the ξ scale, respectively; i.e., the time independent phase factor $[(\xi_0 + \xi_i)\kappa]$ does not contribute to $|\mathcal{C}(\kappa, t)|$.

The situation for case (**II**) is different. The concentration profile in the presence of a reflecting wall at $\xi = 0$ has the form of

$$C(\xi, t)\begin{cases} = 0 & \xi < 0 \\ \neq 0 & \xi \geqslant 0 \end{cases} \qquad [12]$$

and fulfills the boundary condition $(\partial C/\partial x)|_{x=0} = 0$. Since only $\cos \kappa\xi$ (and not $\sin \kappa\xi$) obeys this boundary condition, the (cosine) FT of the concentration profile must be a real function. In practice, a Fourier transform realized through the fast-Fourier-transform (FFT) routine introduces a periodicity (*5, 6*). Thus the FFT of $C(\xi, t)$[11] yields both real and imaginary parts for $\mathcal{C}(\kappa, t)$, but the real part of the FFT is just the same as the *cosine* FT. Thus we may write

$$\ln\left\{\frac{\text{Re}\mathcal{C}(\kappa, t_i)}{\text{Re}\mathcal{C}(\kappa, t_j)}\right\} = -4\pi^2 D_\xi t\kappa^2. \qquad [13]$$

A problem appears when the reflecting wall and/or the reference spectrum is displaced along ξ. Such displacements introduce κ-dependent phase factors in Fourier space, which contribute to the real and imaginary parts of the FFT of $I_g(\xi, t)$: $\mathcal{I}_g^d(\kappa, t) = \mathcal{C}(\kappa, t)e^{2\pi j\xi'\kappa} \cdot \mathcal{I}_0(\kappa)e^{2\pi j\xi''\kappa} = \mathcal{C}(\kappa, t)e^{2\pi j\xi_0\kappa}\mathcal{I}_0(\kappa)$, ξ' and ξ'' are displacements of $C(\kappa, t)$ and $I_0(\xi)$, respectively, and superscript d refers to the result of displaced functions. Thus, in order to extract $\text{Re}\mathcal{C}(\kappa, t)$ both real and imaginary parts of $\mathcal{C}^d$ must be taken into account, and Eq. [13] takes the form of

$$\ln\left\{\frac{\cos \kappa\xi_0 \cdot \text{Re}\mathcal{C}^d(\kappa, t_i) + \sin \kappa\xi_0 \cdot \text{Im}\mathcal{C}^d(\kappa, t_i)}{\cos \kappa\xi_0 \cdot \text{Re}\mathcal{C}^d(\kappa, t_j) + \sin \kappa\xi_0 \cdot \text{Im}\mathcal{C}^d(\kappa, t_j)}\right\} = -4\pi^2 D_\xi t\kappa^2, \qquad [14]$$

where $\mathcal{C}^d(\kappa, t) = \mathcal{I}^d(\kappa, t)/\mathcal{I}_0(\kappa)$. Since $\xi_0 = \xi' + \xi''$ is the relative mismatch between the positions of the wall and of the center of the reference spectrum, the phase factor can be interpreted as resulting from shifting either the reflective wall or the reference spectrum. Experimentally accounting for ξ_0 through Eq. [14] cannot be accom-

plished easily and, instead, alignment of the reflecting wall with the reference spectrum is advisable (*2*).

IMPROVEMENTS IN DID-ESR TECHNIQUE

In our previous paper (*2*) we gave technical details of the DID-ESR experiment in the geometries of unrestricted and restricted diffusion and a detailed discussion of different variants of the numerical data analysis. In particular, it was shown that it is possible to prepare a sufficiently narrow and symmetric initial distribution to obtain Gaussian character of the concentration profiles at a later time for both geometries, (**I**) and (**II**), thus making either Eq. [10] or Eq. [13] applicable. Subsequently, the unrestricted geometry was successfully applied to study lateral diffusion in model membranes (*2, 3*).

Despite this success, we also pointed out difficulties and limitations of the experiment and data analysis. In particular, we have found that when performing an experiment in the presence of the reflective wall, it is essential for accurate determination of the diffusion coefficient to precisely align the reflecting boundary and the center of the cavity. Otherwise, a cumbersome data manipulation is necessary, increasing the uncertainty of D_x value (*2*). We have shown also that the data analysis in Fourier space must be restricted to a limited range of κ, $\kappa_{\min} < \kappa < \kappa_{\max}$, due to the presence of random noise in the data and round-off errors of numerical calculations.

In this section we present a convenient way of optimizing the accuracy of estimation of D_x, which effectively removes the earlier arbitrariness of choosing an appropriate range of κ values suitable for analysis. We will also show how, with this new procedure of dealing with the data, the mechanical alignment of the reflective boundary with the center of the cavity in the restricted geometry can be replaced by a simple magnetic field adjustment or numerical alignment of digitized I_g and I_0 spectra.

Improved estimation of D_ξ. As a result of random errors in the value of $\ln[\mathcal{C}(\kappa, \tau_i)/\mathcal{C}(\kappa, \tau_j)]$, the linearity with respect to either κ^2 or $\Delta t_{ij}\kappa^2$ is observed over only a limited range of κ, $\kappa_{\min} < \kappa < \kappa_{\max}$. The lower limit is a result of very small differences between concentration profiles from different times at low κ, which are of the order of the random error. The upper limit reflects the fact that at high κ the magnitudes of the $\mathcal{C}(\kappa, t)$ are themselves becoming very small (*2*). Estimation of D_ξ previously had, therefore, some degree of arbitrariness, associated with the freedom of choosing $\kappa_{\min}$ and $\kappa_{\max}$. To reduce this arbitrariness, we propose the following simple procedure. The diffusion coefficient is calculated from the data with different ranges of consecutive κ values taken into account. The calculated diffusion coefficient (D_{slope}) is then a function of the range of κ that is taken into account, ($\kappa_{\min}$, $\kappa_{\max}$), $D_{\text{slope}} = D_{\text{slope}}(\kappa_{\min}, \kappa_{\max})$. However, we found that if $\kappa_{\min}$ is small, D_{slope} is rather insensitive to its value. Then let $\kappa_{\min}$ be small and fixed so D_{slope} is only a function of $\kappa_{\max}$. For small values of $\kappa_{\max}$ ($\geqslant \kappa_{\min}$), D_{slope} should initially have erratically scattered values. However, as $\kappa_{\max}$ increases it should go through a *plateau* corresponding to D_ξ. On further increase in $\kappa_{\max}$, the random scatter of data points at higher κ should force the D_{slope} to deviate (decrease) significantly again. Clearly, an immediate advantage of such analysis of calculated values of D_{slope} is (i) the removal of the aforementioned arbitrariness in choosing the cut-off limits for κ, and (ii) an instant readout of the D_ξ value from the plot.

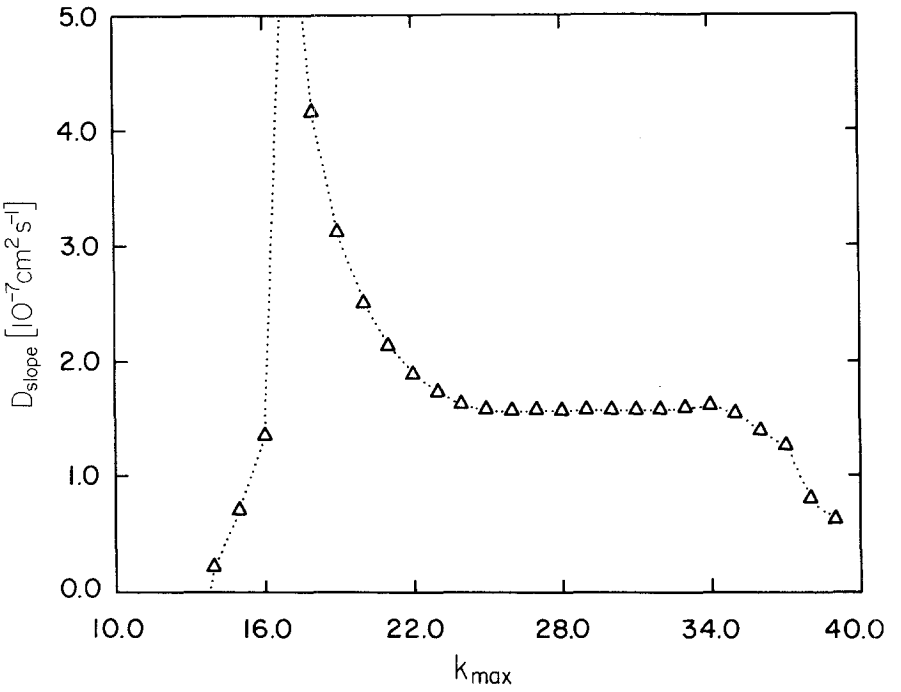

FIG. 1. $D_{slope}(k_{max})$ plot for geometry of unrestricted diffusion; k_{max} is in units of cm^{-1}. (CSL spin probe in an oriented model membrane of POPC at 333 K.)

To demonstrate the effectiveness of this procedure we have applied it to our recent measurements of the translational diffusion of CSL spin probe in an oriented model membrane of POPC (*3*), see Fig. 1. The presence and extent of the plateau are clearly visible. Note that fluctuations in values of D_{slope} at the plateau are extremely small. We may then state that the plateau in $D_{slope}(\kappa_{max})$ singles out the most probable value of the diffusion coefficient, D_ξ.

We will show now how the plot of $D_{slope}(\kappa_{max})$ can significantly assist the experiment as well as improve the data analysis in the presence of the reflective wall.

Improved experiment with the reflective boundary. We found experimentally in the past that, in the presence of a reflective wall, the analysis of experimental data runs into difficulty when trying to deconvolute the concentration profile from I_g and I_0 spectra. The successful deconvolution was possible only when the reflective boundary had been placed precisely in the center of the cavity (*2*).

The origins of this difficulty can be explained as follows. Let a sample with a reflective boundary be present in the cavity and let ξ_0 correspond to the center value of the static field in the absence of the magnetic field gradient. The signal is recorded only over some limited sweep range of the static magnetic field (i.e., $\pm\frac{1}{2}$, since the sweep range in dimensionless units is just 1) around the center field value (ξ_0). Thus the particular position of the ESR spectrum inside this "window" depends on the value of ξ_0. The spectrum recorded under these conditions is our reference one (I_0), and we may consider ξ_0 as the reference point (origin) on the ξ scale. Next, the magnetic

field gradient is switched on. In general, the static magnetic field at the position of the reflecting wall is changed because of the gradient, so there is a *mismatch* between the position of the reflective wall and the reference point on the ξ scale. Consequently, the gradient-on spectrum is the convolution of the concentration profile and the *shifted* reference spectrum, and the corresponding Fourier transform contains a κ-dependent phase factor reflecting this misalignment, cf. Eq. [14].

In order to perform a successful deconvolution of the concentration profile we must, therefore, counteract the mismatch either prior to or after FT. The latter choice of correcting the phase factor in Fourier space is more cumbersome and unreliable and we refrained from using it in the past. We now point out that corrections prior to FT offer much more convenient and elegant options. These corrections can be performed by adjustments in x, B, and ξ spaces, since they are equivalent. To do a proper adjustment we need, however, a reliable method of controlling "alignment." We describe below the principles of monitoring the alignment of the spectra.

Most frequently an ESR spectrum is detected as the first derivative of the absorption,

$$\begin{aligned} I'_g(\xi) = \frac{dI_g}{d\xi} &= -\int_0^\infty C(\xi')\frac{dI_0(\xi-\xi')}{d\xi'}\,d\xi' \\ &= -C(\xi')I_0(\xi-\xi')\Big|_{\xi'=0}^{\xi'=\infty} + \int_0^\infty \frac{dC(\xi')}{d\xi'} I_0(\xi-\xi')d\xi' \\ &= C(0)I_0(\xi) + \int_0^\infty \frac{dC(\xi')}{d\xi'} I_0(\xi-\xi')d\xi', \end{aligned} \qquad [15]$$

where we assumed that the reflective wall is present at $\xi = 0$, cf. Eq. [12]: Note that the first term on the right hand side of Eq. [15] is just the absorption spectrum scaled by the factor $C(0)$. Let us assume for a moment that $I_0(\xi)$ is a singlet. Then, because $dC/d\xi$ is either zero or very small (negative) in value in the vicinity of the reflecting wall (recall the boundary condition, $(\partial C/\partial\xi)|_{\xi=0} = 0$), the first term on the right hand side dominates the spectrum around $\xi = 0$. We may then state that this (sharp) maximum corresponds to the position of the reflective wall on the ξ scale. Similarly, for the double- or triple-line reference spectrum, like ^{15}N or ^{14}N nitroxide spin labels, as a result of the presence of the reflective boundary, $I'_g(\xi)$ should feature maxima uniquely corresponding to the reference spectrum lines. Therefore, to fulfill the requirement of a proper deconvolution via FFT, both spectra, I'_g and I_0, must be aligned in such a way that positions of sharp maxima in I'_g coincide with centers of I_0 lines (or the crossover points in the first derivative spectrum, I'_0), see Fig. 2. This alignment can be achieved either by varying the position of the reflective wall inside the cavity or by changing the static magnetic field between recording I'_g and I'_0, in the following way. The first-derivative spectra of gradient-*on* and gradient-*off* are first recorded and their positions on the recording chart compared. If they do not match each other, adjustment is necessary and this can be done two ways. First, we can repetitively move the position of the reflective wall inside the cavity, record I'_0, and check again if satisfactory alignment was achieved. Alternatively, we can obtain the alignment by varying not the position of the wall but the position of I'_0 through

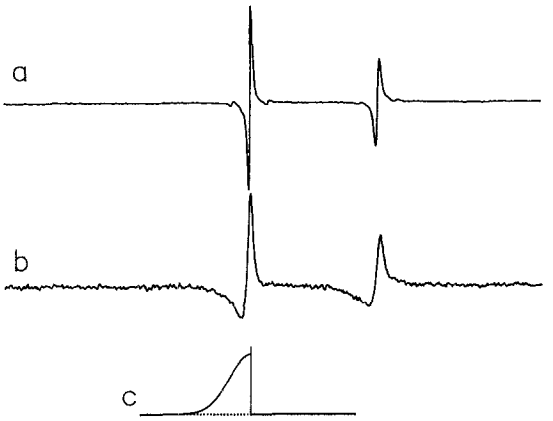

FIG. 2. Adjusted first-derivative (a) gradient-*off* and (b) gradient-*on* spectra in the presence of a reflective wall. Adjustment was made by varying the static magnetic field prior to recording the gradient-*off* spectrum. Schematically shown in (c) is the position of the reflective wall and the concentration profile. (MBBA with ^{15}N-PDT spin probe at room temperature. Sweep range 200 G.)

changes of the static magnetic field. It is, however, very difficult to judge when we have achieved satisfactory alignment.

The spectral alignment can be very precisely monitored with the aid of the D_{slope} vs $k_{\max}$ plot (note $k = \kappa \cdot B'/B_s$). In the case of a perfect match between the spectra, D_{slope} must go through a plateau over the ($k_{\min}$, $k_{\max}$) range, the D_{slope} value at the plateau corresponding to D_x, the same way as it does for the unrestricted diffusion experiment, Fig. 1. In the presence of a mismatch between spectra, a k-dependent phase factor appears in $\mathcal{C}(k, t)$, and the plateau disappears even for a very slight displacement. To illustrate this, we carried out test measurements of the diffusion coefficient of a spin probe (^{15}N-PDT) in the nematic phase of MBBA at room temperature. Measurements were performed on the same experimental setup as described earlier (*2*), but with a new source of the magnetic field gradient (a pair of George Associates Lewis Coils, Model 502). For the purpose of measurements a cell was made from a square 0.4×0.4 cm^2 quartz tube, approximately 10 mm in length and attached axially to a supporting glass rod. The spin-label-enriched material can then be placed in a form of a thin film on one of the sidewalls of the cell so the distance available for diffusion is about 0.4 cm. After deposition, the enriched material was solidified and the cell filled with pure MBBA. The sample was next allowed to thermally equilibrate over a period of a few minutes. The sample was placed inside the cavity with a standard sample mount, and by rotating the support rod the reflective wall oriented either parallel or perpendicular to the static magnetic field. Note that because of the axial symmetry of the cell, the reflecting wall is off the center and mechanical adjustments of its position are impossible.

First, a series of 20 gradient-on spectra were recorded at different times. Next, a few I'_0's were recorded for slightly different values of the central field ($\sim$0.1–0.2 G) chosen so that the spectral alignment of I'_0 and I'_g seemed close to perfect. Different concentration profiles were paired and the mean $D_{\text{slope}}(k_{\max})$ was calculated for each I'_0 recorded, see Fig. 3a. As expected, a relatively small departure of I'_0 from perfect

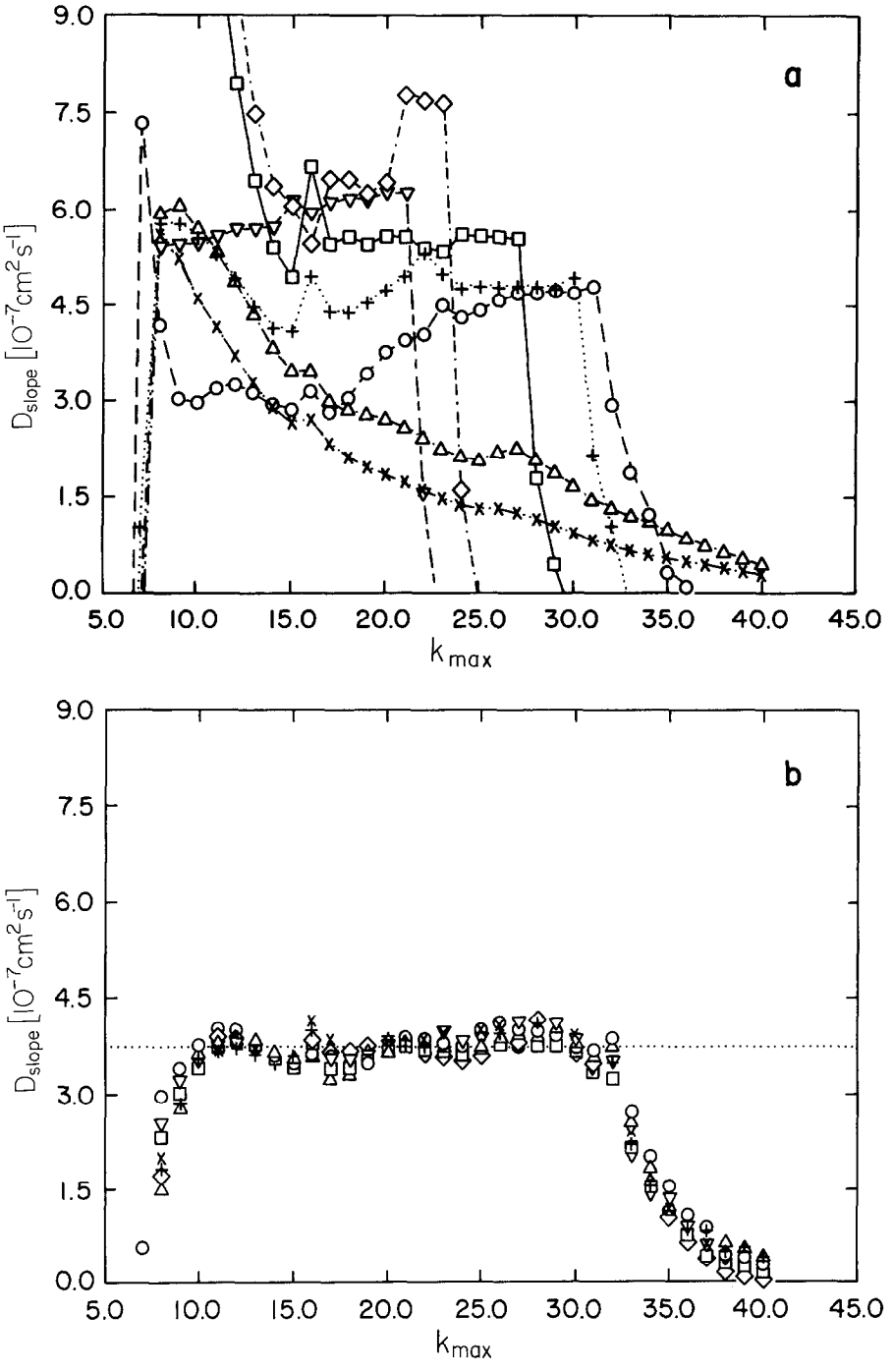

FIG. 3. Diffusion perpendicular to B_0, in the presence of a reflective wall. $D_{slope}(k_{max})$ for a number of $I_0(B)$ spectra slightly (but differently) displaced with respect to $I_g(B, T)$: (a) raw data without numerical adjustment; (b) the same data but after numerical adjustment; dotted straight line indicates the average value of D_{slope} at the plateau; k_{max} is in units of cm^{-1}. (MBBA with ^{15}N-PDT spin probe at room temperature.)

alignment with I'_g not only inclines the plateau, upward (downward) due to the I'_0 shift to the left (right) from perfect alignment, but it also makes the estimation of D unreliable. The existence of the plateau is, therefore, a reliable criterion for the quality of spectral alignment.

If the recorded spectra do not produce a reliable plateau, further adjustments are necessary. This can be done in an elegant way by a careful *numerical* shift of the $I'_0(\xi)$ spectrum along the ξ axis. The results of such manipulations of the experimental data from Fig. 3a are shown in Fig. 3b. Clearly, we were able to adjust all recorded spectra to obtain essentially the same plateau. It must be noticed, however, that fluctuations in D_{slope} are more pronounced than in the case of unrestricted diffusion, cf. Fig. 1, substantially reducing the precision of D_x that is determined with the restricted geometry of diffusion.

LIMITS AND ERRORS OF THE DID-ESR EXPERIMENT

In our previous work (*2, 3*) we have shown experimentally that within an hour it is possible to measure a diffusion coefficient as small as a few 10^{-8} cm^2 s^{-1}, using a standard ESR spectrometer and Fourier-domain analysis. We did not, however, attempt to estimate either the smallest or the largest diffusion coefficient measurable by DID-ESR, nor the uncertainty of the determined value of D_x, and we would like to address these problems in this section.

There are numerous potential sources of errors in the DID-ESR experiment, so before going into any quantitative discussion we will first try to identify the most influential ones. Furthermore, we will concentrate only on those effects which cannot be eliminated by careful tuning of the equipment and, therefore, are inherent to the experiment. Some of these effects are characteristic of ESR spectroscopy in general, while the others can be associated with particular features of the DID-ESR experiment. The first group includes such obvious effects as the noise, nonuniform sensitivity of the cavity, or inhomogeneous static magnetic field. To the second group belong such effects as a nonuniform magnetic field gradient, finite sweep time, poorly defined initial concentration profile, or nonideal boundary conditions for diffusion. Some of these effects are mainly responsible for systematic errors, and others cause random errors in D_x. Let us begin with the potential sources of the systematic errors, since they determine, first of all, the credibility of the DID-ESR technique.

The most natural way in which *systematic errors* will manifest their presence is in a nonlinear behavior of $\ln[\mathcal{C}(\kappa, t_i)/\mathcal{C}(\kappa, t_j)]$ as a function of κ^2, cf. Eq. [7]. Such nonlinearity can rise, first of all, from poorly defined initial distribution and should be most prominent in measurements performed shortly after initialization of the diffusion (the rapid measurement). With passing time, however, the difference between the actual concentration profile and the Gaussian shape should become negligible as a result of the diffusion, leading to the disappearance of any nonlinearity. To confirm this, we studied the problem numerically, and a number of simple simulations were performed. Different shaped initial distributions were tried: a layer-like distribution with thickness of $2\xi_0$, i.e., spin probes are confined in the region $-\xi_0 < \xi < \xi_0$, as well as more complicated, but realistic, distributions. Simulations confirmed the importance of keeping the breadth of the initial distribution as narrow as possible,

although they revealed that the initial shape of the distribution is not as significant as one might expect, as long as the shape is kept reasonable, e.g., thin film or globular droplet. No systematic deviations between estimated and assumed values of D_ξ were observed, and discrepancies were within the accuracy of the calculations. If sufficient time was "allowed" for profiles to develop, e.g., when $D_\xi t > 2\xi_0$, concentration profiles become very close to the Gaussian function, as expected. We concluded, therefore, that a poorly prepared initial distribution can be a source of systematic error only at the early stages of the experiment. In practice a poor initial distribution can be easily recognized at the start of an experiment and discarded.

Nonuniformity of the field gradient and a position-dependent sensitivity of the cavity are other possible sources of the nonlinearity of $\ln[\mathcal{C}(\kappa, t_i)/\mathcal{C}(\kappa, t_j)]$ as a function of κ^2. If the cavity sensitivity $S(\xi)$ varies with position, then the effective concentration profile "seen" by the DID-ESR technique is the product of $S(\xi) \cdot C(\xi, t)$, and this should lead to difficulty in the determination of D_x in Fourier space. If the variation of $S(\xi)$ is small, one must expect a small but systematic deviation of the estimated value from the "true" one. The deviation can be to some extent compensated if the sensitivity dependence on position in the cavity is known (*1*), but the analysis is not an easy task and increases the uncertainty of D_ξ. Strongly inhomogeneous sensitivity essentially excludes the possibility of a precise measurement of D_ξ altogether. Our experience with the narrow-flange TE_{102} X-band microwave resonance cavity shows that the sensitivity of the cavity did not influence results as long as the concentration profile was confined to ±5 mm around the center of cavity.

The effect of a nonuniform gradient is similar. Such a gradient would produce a nonlinear mapping of x space onto B space, violating the basic assumptions of the method, and thereby, at best, reducing the accuracy of the method. It is, therefore, essential to perform test measurements of the uniformity of the gradient, each time the gradient coils are moved. We found in the past that the coils we have employed produce a uniform gradient over the whole region where the sensitivity is sufficiently homogeneous for DID-ESR measurements (*1*). Nevertheless, we must stress that an inhomogeneity in the sensitivity and nonlinearity of the gradient can produce time-dependent deviations which are difficult to account for quantitatively. Therefore, one must take pains to ensure that the sensitivity and the gradient are as uniform as possible.

Until this point, we have been implicitly assuming that there is instantaneous detection of the ESR spectrum, particularly the I_g spectrum. The recording time (= sweep time) is, however, finite, and the above assumption is valid only as long as the spectrum can be considered time independent over the time of sweep through the spectrum. Unfortunately, under standard experimental conditions, the sweep time may be sufficiently long to distort the shape of the spectrum recorded, thus also that of $\mathcal{C}(\kappa, t)$. Let the sweep rate be v_s and the sweep-time t_s: then $v_s t_s = 1$ (we recall that in dimensionless units the sweep range is 1). Let us also assume for simplicity that the concentration profile is a Gaussian centered at $\xi = 0$,

$$C(\xi, t) = \frac{C_0}{\sqrt{2\pi\sigma_\xi^2(t)}} \exp\left\{-\frac{1}{2}\frac{\xi^2}{\sigma_\xi^2(t)}\right\}$$

$$= \frac{C_0}{\sqrt{2\pi(\delta_0^2 + 2D_\xi t)}} \exp\left\{-\frac{1}{2}\frac{\xi^2}{\delta_0^2 + 2D_\xi t}\right\}, \qquad [16]$$

where σ_ξ^2 is the variance of the concentration profile (the HWHW is approximately

equal to $1.18\sigma_\xi$), δ_0^2 is the variance of the initial distribution, and t is measured from the moment of initialization of the diffusion. Then, by simple substitution, we find that the original Gaussian profile will be skewed by the recording procedure:

$$\exp\left\{-\frac{1}{2}\frac{\xi^2}{\delta_0^2+2D_\xi t}\right\} \overset{\text{sweep}}{\Rightarrow} \exp\left\{-\frac{1}{2}\frac{\xi^2}{\delta_0^2+2[D_\xi\{1+\xi/(tv_s)\}]t}\right\}. \quad [17]$$

Because ξ changes sign in the course of the sweep, one-half of the recorded curve is compressed, while the second half stretched with respect to the original Gaussian distribution, the degree of the distortion being inversely proportional to v_s. Equation [17] may be thought of as the imaging analog of the Doppler effect. If the distortion is not too large and both parts of the distribution, the compressed and stretched, can be approximated by Gaussian curves with σ_-^2 and σ_+^2, respectively, then one can approximate the variance of the skewed distribution which by definition is (7)

$$\begin{aligned}\tilde{\sigma}_\pm^2 &\simeq (\sigma_-^2+\sigma_+^2)/2\\ &= [\delta_0^2+(D_\xi/v_s)^2 4\ln 2]+2D_\xi t\\ &\equiv \delta_0'^2+2D_\xi t.\end{aligned} \quad [18]$$

Thus, provided that $2D_\xi t_s \ll (\delta_0^2+2D_\xi t)$, the artificial broadening caused by the sweep is negligible and therefore should not lead to a systematic error. To fulfill this requirement, one should then keep $v_s t$ as large as possible, which means either fast sweep rates or large t (broad distributions).

Unfortunately, the last statement refers to unrestricted diffusion only. In the presence of a reflective wall, one gets either the compressed or the stretched concentration profile depending on the direction of the sweep, $\sigma_-^2 < \sigma_+^2$, leading to under- or overestimation of the diffusion coefficient, respectively. By careful choice of the sweep time, we can, nevertheless, reduce this systematic error to a minimum. For example, if we want sweep-related errors smaller than 2%, for an initial distribution width of 0.02 cm and D_x of order of 10^{-8} cm^2 s^{-1}, the sweep time should be faster than 0.05 s for a measurement performed shortly after initialization of the diffusion (rapid measurement) and faster than 50 s for a measurement with a concentration profile significantly broadened by the diffusion (delayed measurement). In principle, this problem may also be overcome by consecutive measurements of σ_-^2 and σ_+^2 with averaging of these two values.

At this point we must emphasize that a combination of the restricted space available for diffusion, introduced by the inhomogeneous sensitivity of the cavity, and of restrictions due to the finite sweep time sets the *upper limit* on the measurable diffusion coefficient under given experimental conditions. In order to estimate this limit, we need to consider the broadest concentration profile measurable, since this would guarantee the minimum error associated with the sweep time in any circumstances, cf. Eq. [17]. The maximum measurable breadth of the concentration profile is solely defined by the extent of the region where the sensitivity can be considered uniform. For the narrow-flange TE_{102} cavity, or a typical loop–gap resonator, this corresponds to about $x_{max} \simeq 0.5$ cm from the center. Precise measurement of the concentration profile is possible as long as most spin probes remain in this region. It is difficult to estimate how many spin probes should remain there, but let us again benefit from

well-known properties of the normal (Gaussian) distribution. If the concentration profile is Gaussian then, for example, $3\sigma_x \leqslant x_{max}$ would guarantee that only a fraction of a percent (less than 0.27%) of spin probes has left the region. For such a concentration profile, distortions from the sweep would be avoided if the diffusion coefficient obeys the inequality, $2D_x t_s \ll (x_{max}/3)^2$, which for a typical sweep time of 60 s becomes $D_x \ll 2 \times 10^{-4}$ cm^2 s^{-1}. We may then stipulate that it should be possible to measure diffusion as fast as 10^{-5} cm^2 s^{-1} with the unrestricted geometry. When the reflecting wall is present, as a result of compressing or stretching the profile by the sweep, the maximum measurable diffusion coefficients should be smaller than this estimated limit.

Due to our interest in studying translational diffusion in liquid crystals and model membranes, where typical diffusion coefficients are of the order of 10^{-6}–10^{-10} cm^2 s^{-1} (*8, 9*), we are primarily concerned with the *lower limit* of measurable D_x values. This question would not be complete, however, without specifying the time period, t_D, in which we would like to measure the diffusion constant. Clearly, extending the time of the experiment to infinity, we should be able, in principle, to measure infinitely small diffusion constants, but, in practice, we are interested in keeping the time of measurement as long as possible but within reasonable limits. We found experimentally that an hour is a reasonable choice for a single measurement, $t_D \simeq 1$ h.

As we mentioned already, *random errors* present in the ESR spectra and/or introduced by numerical procedures (round-off errors) limit the range of κ values useful for analysis. To facilitate the estimation of this range, we assume again that the concentration profile is Gaussian and that the $I_0(\xi)$ spectrum is a single unsaturated Gaussian ESR line with the variance of Δ_B^2 (*1*). Then, $\mathcal{J}_g(\kappa, t)$ is just a convolution of two Gaussians, so its image in Fourier space is

$$\mathcal{J}_g(\kappa, t) = A \exp\{-2\pi^2(\Delta_\xi^2 + \delta^2 + 2D_\xi t)\kappa^2\}, \qquad [19]$$

where $A = \int_{-\infty}^{\infty} I_g(\xi, t)d\xi$ and δ^2 denotes now the variance of the concentration profile at the beginning of measurement, and t is measured from the beginning of measurement. Note that, because the ESR linewidth is independent of the magnetic field gradient, the variance of the line in ξ space is $\Delta_\xi^2 = \Delta_B^2/B_s^2$. Next, we assume that the noise in κ space is white noise with a variance of s_κ^2.

Since $\mathcal{J}_g(\kappa, t)$ is a Gaussian, its amplitude decreases with increasing κ, eventually becoming comparable to the noise for some value of $\kappa = \kappa_{max}$: $\mathcal{J}_g(\kappa_{max}, t) \approx s_\kappa$. Therefore, all values of $\mathcal{J}_g(\kappa, t)$ for $\kappa > \kappa_{max}$ will be useless for analysis. Denoting the signal-to-noise ratio in Fourier space by $\epsilon_\kappa = A/s_\kappa$, with the help of Eq. [19] we obtain

$$\kappa_{max}^2 \approx \frac{\ln \epsilon_\kappa}{2\pi^2(\Delta_\xi^2 + \delta^2 + 2D_\xi t)}, \qquad [20]$$

for the *upper* limit of κ values. Since at the beginning of a measurement $t = 0$, then the upper limit is set by the spectrum recorded at $t = t_D$.

The pairing technique on its own imposes a limit on the usefulness of $\mathcal{J}_g(\kappa, t)$ at small values of κ, due usually to very small differences between paired concentration profiles in this range. In order to distinguish between two concentration profiles separated by time t_D, the difference between $\mathcal{J}_g(\kappa, 0)$ and $\mathcal{J}_g(\kappa, t_D)$ at small κ should be at least twice the noise. With the help of Eq. [19] we obtain

$$\frac{|\mathcal{J}_g(\kappa, t_D) - \mathcal{J}_g(\kappa, 0)|}{|\mathcal{J}_g(\kappa, 0)|} \approx \frac{2s_\kappa}{A \exp\{-2\pi^2(\Delta_\xi^2 + \delta^2)\kappa^2\}} \approx 4\pi^2\kappa^2 D_\xi t_D. \quad [21]$$

Thus, from Eq. [21], the *lower* limit of κ values is given by the solution of

$$2\pi^2\epsilon_\kappa D_\xi t_D \kappa_{\min}^2 = \exp\{2\pi^2(\Delta_\xi^2 + \delta^2)\kappa_{\min}^2\}, \quad [22]$$

which, since $(\Delta_\xi^2 + \delta^2)\kappa_{\min}^2$ is small, is approximately

$$\kappa_{\min}^2 \approx \frac{1}{2\pi^2(\epsilon_\kappa D_\xi t_D - \Delta_\xi^2 - \delta^2)}, \quad [23]$$

where we require

$$D_\xi > (\Delta_\xi^2 + \delta^2)/(\epsilon_\kappa t_D), \quad [24]$$

in order that Eq. [23] be physically meaningful.

We optimize the measurement by maximizing the difference $(\kappa_{\max}^2 - \kappa_{\min}^2)$, and this is done through adjustment of the magnetic field gradient, since both D_ξ and δ^2 are proportional to B'^2. The difference is a maximum when the first derivatives of Eqs. [20] and [23] with respect to B'^2 are equal. Using explicitly the variables in x and B space we obtain

$$\frac{\alpha}{\{\alpha B'^2 - \Delta_B^2\}^2} = \frac{\beta \ln \epsilon_\kappa}{\{\beta B'^2 + \Delta_B^2\}^2}, \quad [25]$$

yielding

$$\frac{B'^2}{\Delta_B^2} = \left[\sqrt{\frac{\alpha}{\beta \ln \epsilon_\kappa}} + 1\right]\left[\alpha - \sqrt{\frac{\alpha\beta}{\ln \epsilon_\kappa}}\right]^{-1}, \quad [26]$$

where $\alpha = \epsilon_\kappa D_x t_D - \delta_x^2$ and $\beta = 2D_x t_D + \delta_x^2$. Equation [26] has a physical solution only if $\alpha > 0$, i.e., $D_x > \delta_x^2/(\epsilon_\kappa t_D)$. However, this condition is guaranteed by Eq. [24]. Thus, Eq. [24] sets the lower limit on the measurable diffusion coefficient,

$$D_x > \frac{\Delta_B^2/B'^2 + \delta_x^2}{\epsilon_\kappa t_D}, \quad [27]$$

whereas Eq. [26] yields the optimum gradient, B'. Our spectrometer with our usual samples yields an ϵ_κ of the order of 50, but the half-width of the distribution can be anywhere between $\delta_x \approx 0.04$ cm and $\delta_x \approx (x_{\max}/3)$, where the lower limit is defined by the breadth of a narrow initial distribution and the upper limit corresponds to the size of the sensitive region in the center of cavity. These limits correspond to two particularly interesting applications of the DID-ESR experiment. The first one is a rapid DID-ESR measurement, which for best results should be performed as soon as possible after initialization of the diffusion. The variance of the concentration profile is then essentially equal to that of the initial distribution. The second type of application is in a multiple measurement on the same sample, e.g., temperature-dependent studies, when the last measurement is usually performed on a very broad sample. Usually the ESR lines are narrow, say $2\Delta_B \approx 0.5$ G, and we can safely omit the term Δ_B^2/B'^2 in Eq. [27]. Then, for a one-hour measurement (i.e., $t_D = 4000$) performed

in these two limiting cases, we obtain from Eq. [27] $D_x > 2 \times 10^{-9}$ cm^2 s^{-1} for the rapid measurement and only $D_x > 2 \times 10^{-7}$ cm^2 s^{-1} for a delayed one. The latter limit restricts, therefore, a multiple measurement to cases when the diffusion coefficient is of the order of 10^{-7} cm^2 s^{-1} or higher. The situation worsens, however, if the ESR line is broader, and we must take into account the term Δ_x^2/B'^2 in Eq. [27]. For example, for $\Delta_B \approx 2$ G and $B' = 100$ G cm^{-1} (rapid measurement) we obtain $D_x > 4 \times 10^{-9}$ cm^2 s^{-1}, and for $B' = 10$ G cm^{-1} (delayed measurement) we should expect $D_x > 4 \times 10^{-7}$ cm^2 s^{-1}.

In order to estimate the error in D_ξ, we return to Eq. [7] which is basic for data analysis. In the process of a linear least-squares fit, each point is weighted by the inverse of the variance of $\ln[\mathcal{C}(k, t_i)/\mathcal{C}(k, t_j)]$, which is roughly of the order of $\epsilon_\kappa^2/2$, so the error in D_ξ can be calculated following standard error analysis (7). For typical experimental conditions and for one pair of concentration profiles we estimated the error in D_ξ to be of the order of 10^{-10} s^{-1}. This estimate can be reduced further if we take into account data from a number of pairs. Therefore, we may expect the relative errors in D_x to be 10–20% for diffusion coefficients of the order of 10^{-9} cm^2 s^{-1}, but below one percent for 10^{-7} cm^2 s^{-1}. We note also that for fast diffusion processes, errors arising from B' and B_s can give a substantial contribution to the uncertainty in D_x.

The estimate of error of D_x is valid in both unrestricted and restricted geometries, but we must comment on the fluctuations seen in the plateau of the D_{slope} plot, see Fig. 3b. These fluctuations are due to imperfections either of the reflective wall surface (inhomogeneous boundary conditions at the wall) or in the alignment procedure. If the reflective wall is rough, it produces an uncontrollable local misalignment of the I_g and I_0 spectra at different positions on the wall, introducing a position-dependent k-dependent phase factor leading to "wavy" behavior of the plateau. The second is due to the discrete character of the digitized spectra and to the presence of noise and is responsible for discrepancies between $D_{\text{slope}}(k_{\max})$ curves for different reference spectra. The errors resulting from imperfections of the wall are significantly larger than those from the discrete character of the ξ space and cannot be averaged out by the use of multiple pairs. How critical this contribution can be is clearly seen by comparing Figs. 1 and 3, showing $D_{\text{slope}}(k_{\max})$ in the absence and in the presence of a reflective wall, respectively. The estimated relative standard deviations of D_x are 1 and 5%, respectively. In order to minimize the uncertainty of D_x in the latter case, it is very important to use very good quality (flat) reflecting-wall surfaces, perfectly oriented with respect to the direction of the gradient.

We now calculate the total number of measurements which can be done on the same sample, since this is important for multiple experiments. To simplify calculations, we define t' as the *delay time* between initialization of diffusion and the beginning of the measurement, and t_0 as a hypothetical time in which the initial (Gaussian) distribution would develop from a point source, i.e., $\delta_x^2 \equiv 2D_x t_0$, cf. Eq. [3]. Because this time t_0 is irreversibly lost for measurement, we may call it the *dead time* of the experiment. The variance of the concentration profile, Eq. [16], can be rewritten as

$$\sigma_\xi^2(t) = 2D_\xi t_0 + 2D_\xi t' = 2D_\xi t. \qquad [28]$$

Thus, t should now be considered the *absolute* delay time of the measurement.

At the beginning of each measurement we optimize the sensitivity of the instrument to the value of σ_ξ^2 at that time by an appropriate adjustment of B', so the sensitivity remains optimal in the course of multiple experiment. Let D_ξ denote the value of the diffusion constant at the beginning of the first measurement, i.e., $D_\xi = D_x(B_0'/B_s)^2$, where B_0' is the magnetic field gradient after the first adjustment. Then the variance at the beginning of each measurement can be written as

$$\sigma_\xi^2(t) = 2D_\xi \cdot \left(\frac{t_0}{t}\right) t, \qquad [29]$$

and at the end of this measurement as

$$\sigma_\xi^2(t + t_D) = 2D_\xi \cdot \left(\frac{t_0}{t}\right)(t + t_D), \qquad [30]$$

so the change of the variance over t_D is $\Delta\sigma_\xi^2 = 2D_\xi(t_0/t)t_D$. Notice that since $\Delta\sigma_\xi^2$ remains constant in the course of the multiple experiment, t_D changes from measurement to measurement:

$$\frac{t_D}{t} = \frac{\Delta\sigma_\xi^2}{2D_\xi t_0} = \frac{\Delta\sigma_\xi^2}{\sigma_0^2}. \qquad [31]$$

The absolute delay time after n consecutive measurements, t_n, is

$$\frac{t_n}{t_0} = \left(\frac{\Delta\sigma_\xi^2}{\sigma_0^2} + 1\right)^n = \left(\frac{\Delta\sigma_x^2}{\sigma_x^2} + 1\right)^n, \qquad [32]$$

where we assumed that the diffusion coefficient remains the same over the experiment. Assuming that after t_n the concentration profile has reached the measurable limit, $\sigma_x^2(t_n) \approx (x_{\max}/3)^2$, we calculate the maximum number of single measurements:

$$\begin{aligned} n &\leqslant \ln\left(\frac{t_n}{t_0}\right) - \ln\left(\frac{\Delta\sigma_x^2}{\delta_x^2} + 1\right) \\ &\leqslant 2\ln\left(\frac{x_{\max}/3}{\delta_x}\right) - \ln\left(\frac{\Delta\sigma_x^2}{\delta_x^2} + 1\right). \end{aligned} \qquad [33]$$

For $2x_{\max} \approx 1$ cm, $2\delta_x \approx 0.04$ cm, and a diffusion coefficient of the order of 10^{-7} $\mathrm{cm^2\ s^{-1}}$, we get $n \approx 6$ but for 10^{-6} $\mathrm{cm^2\ s^{-1}}$, only $n \approx 2$. This prediction is in good agreement with our observations (*2, 3*).

CONCLUDING REMARKS

In this paper, which is the third in a series devoted to the development of dynamic imaging of diffusion by ESR (*1, 2*), we described significant improvements in the DID-ESR experiment with the reflective boundary, which make this restricted diffusion geometry a useful alternative to the unrestricted diffusion experiment. We also presented an improved technique of analyzing the data which yields better precision in the determination of diffusion coefficients. We have discussed limits of the DID-

ESR method and shown that at present the DID-ESR technique can be used to study diffusion coefficients in the range 10^{-9}–10^{-5} $cm^2\ s^{-1}$, with precision better than 1% for diffusion constants larger than 10^{-7} $cm^2\ s^{-1}$ and about 10–20% for 10^{-9} $cm^2\ s^{-1}$ based upon a canonical one-hour length of measurement.

As a test of the DID-ESR method with the reflective-wall geometry we have performed translational diffusion measurements of ^{15}N-PDT in the nematic phase of MBBA. The measurements have been carried out at room temperature ($\sim$20°C) on nematic samples oriented parallel and perpendicular to the direction of diffusion. We found coefficients for diffusion parallel and perpendicular to the nematic director equal to $D_l = 3.7 \times 10^{-7}$ $cm^2\ s^{-1}$ and $D_t = 2.5 \times 10^{-7}$ $cm^2\ s^{-1}$, respectively, which yields a D_l/D_t ratio of about 1.5, consistent with existing experimental data for diffusion of other probe molecules in MBBA (*8*). The relative standard deviation (σ_D/D) for diffusion perpendicular (subscript $_t$) to the nematic director was about 5%, and for the parallel direction (subscript $_l$) somewhat larger.

In summary, as a result of improvements described in this paper, the DID-ESR technique is a very simple and reliable experimental method for studying macroscopic translational diffusion.

ACKNOWLEDGMENTS

This work was supported by the NIH under Grant GM-25862 and the NSF under Grants DMR-8604200 and CHE 87-03014. One of us (J.K.M.) acknowledges a partial support of his visit to Cornell University by the Polish Academy of Sciences under Project CPBP 01.12. Dr. R. H. Crepeau is thanked for his comments during preparation of the revised version of this manuscript.

REFERENCES

1. J. P. HORNAK, J. K. MOSCICKI, D. J. SCHNEIDER, AND J. H. FREED, *J. Chem. Phys.* **84,** 3387 (1986).
2. D. A. CLEARY, Y.-K. SHIN, D. J. SCHNEIDER, AND J. H. FREED, *J. Magn. Reson.* **79,** 474 (1988).
3. Y.-K. SHIN AND J. H. FREED, *Biophys. J.* **55,** 537 (1989).
4. J. CRANK, "The Mathematics of Diffusion," Clarendon Press, Oxford, 1976.
5. J. ARSAC, "Fourier Transforms and the Theory of Distributions," Prentice–Hall, Englewood Cliffs, New Jersey, 1966.
6. W. H. PRESS, B. P. FLANNERY, S. A. TEUKOLSKY, AND W. T. VETTERLING, "Numerical Recipes," Cambridge Univ. Press, Cambridge, London/New York, 1986.
7. G. J. KRÜGER, *Phys. Rep.* **82,** 229 (1982).
8. F. NOACK, *Mol. Cryst. Liq. Cryst.* **113,** 247 (1984).
9. S. BRANDT, "Statistical and Computational Methods in Data Analysis," North-Holland, New York, 1970.